

Imprints of dark energy models on structural properties of charged gravastars in extended teleparallel gravity

G. Mustafa,^{1,*} Faisal Javed,^{1,†} Arfa Waseem,^{2,‡} S.K. Maurya,^{3,§} and Ghulam Fatima^{1,¶}

¹*Department of Physics, Zhejiang Normal University, Jinhua 321004, People's Republic of China*

²*Department of Mathematics, Government College Women University, Sialkot, Pakistan*

³*Department of Mathematical and Physical Sciences,*

College of Arts and Sciences, University of Nizwa, Nizwa, Sultanate of Oman

A gravastar comprises three distinct sections: the interior zone, the middle shell, and its outer region. By considering a specific extended teleparallel gravity model that incorporates conformal Killing vectors and provides the field equations. We observe that the interior part exhibits a repellent force acting on the shell. This is based on the assumption that pressure is analogous to negative energy density. The middle shell consists of ultrarelativistic plasma and pressure, which is directly proportional to the matter density and counteracts the repellent force exerted by the inner zone. In the outer zone, we compute the precise solution in a vacuum and then connect these spacetimes using junction conditions to investigate stability limits. We aim to investigate the influence of dark energy models on the stable characteristics of gravastar configurations. It is worth noting that the phantom field exhibits the highest stable configurations for all physically viable selections of physical parameters. We additionally investigate the influence of physical parameters on the correct length, entropy, and energy of the gravastar.

Keywords: Gravastar; modified theory; conformal vectors; stability analysis.

I. INTRODUCTION

The remarkable astrophysical conjecture like gravitational collapse and the exploration of stellar structures have gained the attention of several researchers. Neutron stars, white dwarfs and black holes (BHs) are novel examples of massive as well as dense compact stellar objects that are formed as an outcome of gravitational collapse. In recent years, many authors have suggested that the densest stellar models other than BHs can be produced by the gravitational collapse of a massive star. For this purpose, Mazur and Mottola [1] by incorporating the modified notion of Bose-Einstein condensation in the gravitational field, presented a novel concept of a collapsing celestial body characterized as the gravastar. It is believed that such object coincides with the theoretical conditions for stable stellar development and provides an answer to the issues with classical BHs. In this hypothesis, it is expected that the quantum vacuum oscillations play a major part in the collapsing phenomenon. A phase transformation appears that results in the creation of a repellent de Sitter center, which keeps the collapsing candidate balanced and stops the singularity and horizon from being produced [2]. This conversion occurs very near to the limit $\frac{2m}{r} = 1$, rendering it exceedingly difficult for an outer observer to distinguish between the gravastar and an original BH.

The construction of gravastar structure is specified by three modes in which the inner era ($r \geq 0, r < \mathcal{R}_1$) is based on the isotropic de Sitter center possessing the $p = -\rho$ equation of state (EoS). The outer vacuum era ($r > \mathcal{R}_2$) is displayed through the Schwarzschild metric having $\rho = 0 = p$. The inner and outer modes are isolated by a thin shell ($\mathcal{R}_1 < r < \mathcal{R}_2$) of stiff substance comprising the $\rho = p$ EoS possessing \mathcal{R}_1 as the inner and \mathcal{R}_2 as the outer radius of gravastar. A huge investigation on gravastar geometry has been accomplished after the demonstration of Mazur and Mottola. The stability of gravastar geometry via different EoSs is examined by Visser and Wiltshire [3]. Carter [4] computed the analytical solutions of gravastar and checked the consequences of EoSs on distinct modes of gravastar structure. By taking into account the Born-Infeld phantom in lieu of de Sitter line element, Bilić et al. [5] evaluated the gravastar structures and presented that their outcomes can display the dense dark scenario. Horvat and Ilijić [6] inspected the energy constraints inside the shell of gravastar and analyzed the stable geometry via different techniques. The study of thin-shell gravastars developed from inner de Sitter and outer various BH geometries is presented in [7]-[10].

*Electronic address: gmustafa3828@gmail.com

†Electronic address: faisaljaved.math@gmail.com

‡Electronic address: arfa.waseem@gcwus.edu.pk

§Electronic address: sunil@unizwa.edu.om

¶Electronic address: ghulamfatima.math@gmail.com

Chirenti and Rezzola [11] performed the stability against axial perturbations and found stable structures of gravastar. They also presented the differences of gravastar geometry from BHs. Rocha et al. [12] constructed the models of prototype gravastars and displayed their differences from BHs. Harko et al. [13] considered the accretion disks about slowly rotating gravastars and observed that the thermodynamic as well as electromagnetic attributes of the disks are distinct. They also exhibited that the gravastars yield a less efficient formalism for changing mass to radiation as compared to BHs. In the presence of nonlinear electrodynamics, Lobo and Arellano [14] formed several models of gravastar and examined certain specific features of their structures. Similarly, with the effect of the electric field, Horvat et al. [15] scrutinized the stability of the distinct zones of gravastar. Turimov et al. [16] discussed the outcomes of magnetic field on the structure of gravastar and elaborated the analytical results in the presence of rotation. Javed and Lin [17] explored the gravastar geometry by inducing the quintessence and cloud of strings. The detailed study of thin-shell developing from different inner and outer manifold as studied in [18]-[23].

It is considered that the occurrence of gravitational theories is due to the mysteries behind the cosmological expansion. In such frameworks, the matter and geometry coupling provides various speculations such as $f(R, T)$ theory [24], $f(R, T, R_{\alpha\beta}T^{\alpha\beta})$ theory [25], $f(\mathcal{G}, T)$ [26] and $f(\mathcal{T}, T)$ theory [27] having R as the curvature scalar, T exhibits the trace part of the stress energy tensor, \mathcal{G} indicates the Gauss-Bonnet scalar and \mathcal{T} manifests the torsion scalar. The discussion about the different modes of gravastar geometry has intrigued researchers to scrutinize the impact of different gravitational speculations on the structures of gravastar. In geometry-matter coupled $f(R, T)$ scenario, Das et al. [28] determined the models of gravastar and explored its attributes graphically by incorporating several EoSs. In the light of $f(\mathcal{G}, T)$ conjecture, Shamir and Ahmad [29] derived the singularity-free solutions of gravastar and obtained the expressions of various physical factors. Sharif and Waseem [30] observed the consequences of the Kuchowicz ansatz on the distinct zones of gravastar in $f(R, T)$ gravity. In the light of $f(R, T^2)$ background, Sharif and Naz [31, 32] determined the results of the absence as well as the appearance of electric charge on the geometrical attributes of gravastar. In $f(\mathcal{T}, T)$ theory, Ghosh et al. [33] computed the analytical and singularity free results of the gravastar yielding various physically viable characteristics.

For massive stellar objects, an inherited symmetry having a set of conformal Killing vectors (CKVs) is essential to establish a naturally coherent relationship between the elements of matter and geometry through field equations. These vectors are implemented to provide analytical results of the field equations more accurately as compared to the earlier existing methods. By incorporating such vectors, the giant system consists of nonlinear partial differential equations can be turned into ordinary differential equations. Implementing these KVs, Usmani et al. [34] inspected the various aspects of gravastar by taking into account the electric field and evaluated the solutions for distinct modes of gravastar. Sharif and Waseem [35] scrutinized the significance of the charge factor on the modes of gravastar in the light of $f(R, T)$ scenario by utilizing the CKVs. Bhar and Rej [36] manifested the charged geometry of gravastar with CKV in the light of $f(\mathcal{T})$ conjecture. Sharif et al. [37, 38] investigated the geometry of gravastar without charge and with charge by inducing the CKVs in $f(R, T^2)$ gravity. Ghosh et al. [39] explored the physical characteristics of gravastars solutions in $f(T)$ gravity. The study of gravastars solutions in the framework of branworld gravity is presented in [40] and [41]. Bhar [42] investigated gravastar remedies in the de Rham–Gabadadze–Tolley’s large gravity is similar to that of massive gravity; explore many physical attributes. In the context of $f(Q)$ gravity, we build the non-singular solutions for charged gravastar [43, 44]. Also, the study of charged gravastars in Rastall gravity is presented in [45].

Like other matter-curvature coupled speculations, the $f(\mathcal{T}, T)$ gravity has also gained much attention of researchers in both astrophysical and cosmological scenarios. In this work, we establish the singularity-free results of charged gravastar in the context of $f(\mathcal{T}, T)$ theory with CKV. The paper is organized in such a way that the next section presents the basics of the $f(\mathcal{T}, T)$ scenario. Section III displays the physical exposure of charged gravastars along with the effects of CKVs. Section IV is devoted to matching the exact inner and outer solutions at the intermediate shell to establish the geometry of the gravastar. Then, we scrutinize the impact of phantomlike EoS on the stability of the gravastar model as presented in Section V. The structural attributes like the proper length of the intermediate thin shell, energy contents, and entropy are observed in Section VI. The findings of our work are manifested in the last section.

II. $f(\mathcal{T}, T)$ THEORY

To explore the $f(\mathcal{T}, T)$ theory, we choose the following metric

$$ds^2 = g_{\beta\xi} dx^\beta dx^\xi = \eta_{ij} \theta^i \theta^j, \quad (1)$$

with

$$dx^\beta = e_i^\beta \theta^i; \quad \theta^i = e^i_\beta dx^\beta, \quad (2)$$

where Minkowski metric is described by η_{ij} with $diag(-, +, +, +)$. Further, the expression $e^i{}_\beta$ meets the following relations

$$e_i{}^\beta e^i{}_\xi = \delta_\xi^\beta, \quad e_\beta{}^\xi e^\beta{}_j = \delta_j^\xi. \quad (3)$$

As we are working with the torsional based theory, so the Levi-Civita connection is provided as

$$\dot{\Gamma}^e{}_{\beta\xi} = \frac{1}{2}g^{\rho\sigma}(\partial_\xi g_{\sigma\beta} + \partial_\beta g_{\sigma\xi} - \partial_\sigma g_{\beta\xi}). \quad (4)$$

The Weitzenböck connection or relation is defined as

$$\Gamma_{\beta\xi}^\gamma = e_i{}^\gamma \partial_\beta e^i{}_\xi = -e^i{}_\xi \partial_\beta e_i{}^\gamma. \quad (5)$$

Within the scope of Weitzenböck connection by Eq. (5), the torsion becomes

$$\mathcal{T}_{\beta\xi}^\gamma = \Gamma_{\beta\xi}^\gamma - \Gamma_{\xi\beta}^\gamma. \quad (6)$$

Further, the contorsion tensor is evaluated by

$$K_{\beta\xi}^\gamma = \Gamma_{\beta\xi}^\gamma - \dot{\Gamma}_{\beta\xi}^\gamma = \frac{1}{2}(\mathcal{T}_{\beta\xi}^\gamma + \mathcal{T}_{\xi\beta}^\gamma - \mathcal{T}^\gamma{}_{\beta\xi}). \quad (7)$$

The Eq. (7) can be redefined as

$$K_\gamma{}^{\beta\xi} = -\frac{1}{2}(\mathcal{T}^{\beta\xi}{}_\gamma - \mathcal{T}^{\xi\beta}{}_\gamma + \mathcal{T}_\gamma{}^{\beta\xi}). \quad (8)$$

Th super-potential on combining torsion and contorsion is computed as

$$S_\gamma{}^{\beta\xi} = \frac{1}{2}(K^{\beta\xi}{}_\gamma + \delta_\gamma^\beta \mathcal{T}^{\sigma\xi}{}_\sigma - \delta_\gamma^\xi \mathcal{T}^{\sigma\beta}{}_\sigma). \quad (9)$$

The Lagrangian density for torsion \mathcal{T} expression is given by

$$\mathcal{T} = \mathcal{T}^\gamma{}_{\beta\xi} S_\gamma{}^{\beta\xi}. \quad (10)$$

The Riemann tensor is

$$R_\gamma{}^{\beta\rho\xi} = K_{\beta\rho;\xi}^\gamma - K_{\beta\xi;\rho}^\gamma + K_{\sigma\xi}^\gamma K_{\beta\rho}^\sigma - K_{\sigma\rho}^\gamma K_{\beta\xi}^\sigma. \quad (11)$$

From the above equation, one can evaluate the Ricci scalar as

$$R = -\mathcal{T} - 2D_\beta \mathcal{T}_\xi^{\xi\beta}, \quad (12)$$

where D_β is a covariant derivative. A standard action [46?] having matter coupling for extended teleparallel gravitational theory is provided as

$$s = \int dx^4 e \left\{ \frac{1}{2k^2} f(\mathcal{T}, T) + \mathcal{L}_{(M)} \right\}, \quad (13)$$

where $e = \det(e^i{}_\beta) = \sqrt{-g}$ and $k^2 = 8\pi G$. $\mathcal{L}_{(M)}$ provides the Lagrangian density. The field equations from the Eq. (13) are calculated as

$$\begin{aligned} \frac{8\pi G}{2} T_X^Y &= S_\beta{}^{\xi\rho} (f_{\mathcal{T}\mathcal{T}} \partial_\rho \mathcal{T} + f_{\mathcal{T}T} \partial_\rho T) + [e^{-1} e^i{}_\beta \partial_\rho (e e_i{}^\gamma S_\gamma{}^{\xi\rho}) \\ &+ \mathcal{T}_{\gamma\beta}^\gamma S_\gamma{}^{\xi\rho}] f_{\mathcal{T}} + \frac{1}{4} \delta_\beta^\xi f + \frac{1}{2} f_T (T_X^Y + p_t \delta_\beta^\xi), \end{aligned} \quad (14)$$

where $f_{\mathcal{T}T} = \frac{\partial^2 f}{\partial \mathcal{T} \partial T}$ and $f_{\mathcal{T}} = \frac{\partial f}{\partial \mathcal{T}}$, $f_T = \frac{\partial f}{\partial T}$. On plugging Eq. (11) and Eq. (12) in Eq. (14) the field equations become

$$\left(R_{\beta\xi} - \frac{1}{2} g_{\beta\xi} R \right) f_{\mathcal{T}} + \frac{1}{2} g_{\beta\xi} (f - f_{\mathcal{T}} \mathcal{T}) + 2S_\xi \beta{}^\sigma (f_{\mathcal{T}\mathcal{T}} \nabla_\sigma \mathcal{T} + f_{\mathcal{T}T} \nabla_\sigma T) = (8\pi G - f_T) \mathcal{T}_{\beta\xi} - f_T g_{\beta\xi} p_t. \quad (15)$$

In order to complete this analysis, the following line element is considered

$$ds^2 = -e^{X(r)} dt^2 + e^{Y(r)} dr^2 + r^2 d\theta^2 + r^2 \sin^2 \theta d\phi^2, \quad (16)$$

For the isotropic fluid source, the energy-momentum tensor reads as

$$T_{ij} = \text{diag}(e^X \rho, e^Y p, r^2 p, r^2 p \sin^2 \theta). \quad (17)$$

Being modification in matter part, the electromagnetic stress-energy tensor $E_{i\nu}$ is defined by

$$E_{ij} = 2(F_{i\zeta} F_{j\zeta} - \frac{1}{4} g_{ij} F_{\zeta\chi} F^{\zeta\chi}), \quad (18)$$

where

$$F_{ij} = \mathcal{A}_{i,j} - \mathcal{A}_{j,i}.$$

Further, a tensor, i.e., F_{ij} is expressed in the following form

$$F_{ij,\zeta} + F_{\zeta i,j} + F_{j\zeta,i} = 0, \quad (19)$$

$$(\sqrt{-g} F^{ij})_{,j} = \frac{1}{2} \sqrt{-g} j^i. \quad (20)$$

Now, the Eq. (18) gives us the following relation of electric field (E).

$$E(r) = \frac{1}{2r^2} e^{X(r)+Y(r)} \int_0^r \sigma(r) e^{Y(r)} r^2 dr = \frac{q(r)}{r^2}. \quad (21)$$

In the above equation, $q(r)$ and δ define the total charge as well as the charge density for the system, respectively. Finally, the diagonal tetrad is computed by

$$e_{\gamma}^Y = \left(e^{\frac{X(r)}{2}}, e^{\frac{Y(r)}{2}}, r, r \sin \theta \right). \quad (22)$$

The determinant of e_{γ}^Y yields $e = e^{X(r)+Y(r)} r^2 \sin \theta$. The torsion \mathcal{T} becomes

$$\mathcal{T}(r) = \frac{2e^{-Y(r)}}{r} \left(X'(r) + \frac{1}{r} \right). \quad (23)$$

As, we are working with the diagonal tetrad, a suitable choice of model for $f(\mathcal{T}, T)$ theory [46?] is presented as:

$$f(\mathcal{T}, T) = \alpha \mathcal{T}(r) + c_1 T + c_2, \quad (24)$$

where α , c_1 and c_2 are functional parameters. By using Eq. (16), Eq. (22), and Eqs. (23-24) in Eq. (15), one can get the $f(\mathcal{T}, T)$ field equations as

$$\begin{aligned} 8\pi\rho = & -\frac{e^{-Y(r)}}{4(c_1-1)(c_1+2)r^2} \left(2\alpha c_1 - 4\alpha + \alpha c_1 r^2 Y'(r) X'(r) - 2\alpha \right. \\ & \times c_1 r^2 X''(r) - \alpha c_1 r^2 X'(r)^2 + c_1 r^2 c_2 e^{Y(r)} + 2r^2 c_2 e^{Y(r)} - \alpha c_1 r \\ & \left. \times Y'(r) - 2\alpha c_1 e^{Y(r)} - 3\alpha c_1 r X'(r) + 4\alpha r Y'(r) + 4\alpha e^{Y(r)} \right), \end{aligned} \quad (25)$$

$$\begin{aligned} 8\pi p = & \frac{e^{-Y(r)}}{4(c_1-1)(c_1+2)r^2} \left(2\alpha c_1 - 4\alpha + \alpha c_1 r^2 Y'(r) X'(r) - 2\alpha \right. \\ & \times c_1 r^2 X''(r) - \alpha c_1 r^2 X'(r)^2 + c_1 r^2 c_2 e^{Y(r)} + 2r^2 c_2 e^{Y(r)} + 3\alpha c_1 \\ & \left. \times r Y'(r) - 2\alpha c_1 e^{Y(r)} + \alpha c_1 r X'(r) + 4\alpha e^{Y(r)} - 4\alpha r X'(r) \right), \end{aligned} \quad (26)$$

$$\begin{aligned} 8\pi p = & \frac{e^{-Y(r)}}{4(c_1-1)(c_1+2)r^2} \left(\alpha r^2 Y'(r) X'(r) - 2\alpha c_1 - 2\alpha r^2 X''(r) \right. \\ & - \alpha r^2 X'(r)^2 + c_1 r^2 c_2 e^{Y(r)} + 2r^2 c_2 e^{Y(r)} + \alpha c_1 r Y'(r) + 2\alpha c_1 \\ & \left. \times e^{Y(r)} - \alpha c_1 r X'(r) + 2\alpha r Y'(r) - 2\alpha r X'(r) \right). \end{aligned} \quad (27)$$

An efficient way to use the field equations to follow the natural link between matter and geometry is to employ inheritance symmetry. Typically, inheritance symmetry is used to measure the symmetry resulting from the conformal Killing vectors. Moreover, we employ the vector field h , which may be represented as follows, to further utilize the idea of conformal symmetry

$$\mathfrak{L}_Z g_{XY} = h(r)g_{XY}, \quad (28)$$

where \mathfrak{L} represents the Lie derivative and vector field is denoted by $h(r)$. Using Eq.(16) in Eq.(28), one can get following relations

$$Z^1 X'(r) = h(r), \quad Z^1 = \frac{rh(r)}{2}, \quad Z^1 Z'(r) + 2Z^1_{,1} = h(r).$$

The solutions of this system within the scope of Eq. (16) yield the following expressions

$$e^{X(r)} = K_1 r^2, \quad e^{Y(r)} = \frac{K_2}{h^2(r)}, \quad (29)$$

where, K_1 and K_2 are integration constants. Now, inserting the Eq.(29) in Eqs. (25-27), we attain the modified field equations as:

$$8\pi\rho = \frac{4\alpha(c_1 + 1)h^2(r) + 2\alpha(c_1 + 4)rh(r)h'(r) + K_2(2\alpha(c_1 - 2) - (c_1 + 2)r^2c_2)}{4(c_1 - 1)(c_1 + 2)K_2r^2}, \quad (30)$$

$$8\pi p = \frac{4\alpha(c_1 - 3)h^2(r) - 10\alpha c_1 rh(r)h'(r) + K_2((c_1 + 2)r^2c_2 - 2\alpha(c_1 - 2))}{4(c_1 - 1)(c_1 + 2)K_2r^2}, \quad (31)$$

$$8\pi p = \frac{-4\alpha(c_1 + 1)h^2(r) - 2\alpha(c_1 + 4)rh(r)h'(r) + K_2(2\alpha c_1 + (c_1 + 2)r^2c_2)}{4(c_1 - 1)(c_1 + 2)K_2r^2}. \quad (32)$$

III. CHARGED GRAVASTAR WITH CONFORMAL MOTION

Here, we shall deal with the new charged gravastar solution under conformal symmetry. On using Eq. (29) into Eqs. (30-32) within Eq. (21), one can get the following field equations

$$8\pi\rho + E^2 = \frac{4\alpha(c_1 + 1)h^2(r) + 2\alpha(c_1 + 4)rh(r)h'(r) + K_2(2\alpha(c_1 - 2) - (c_1 + 2)r^2c_2)}{4(c_1 - 1)(c_1 + 2)K_2r^2}, \quad (33)$$

$$8\pi p - E^2 = \frac{4\alpha(c_1 - 3)h^2(r) - 10\alpha c_1 rh(r)h'(r) + K_2((c_1 + 2)r^2c_2 - 2\alpha(c_1 - 2))}{4(c_1 - 1)(c_1 + 2)K_2r^2}, \quad (34)$$

$$8\pi p + E^2 = \frac{-4\alpha(c_1 + 1)h^2(r) - 2\alpha(c_1 + 4)rh(r)h'(r) + K_2(2\alpha c_1 + (c_1 + 2)r^2c_2)}{4(c_1 - 1)(c_1 + 2)K_2r^2}. \quad (35)$$

$$(36)$$

The expressions of physical factors are obtained simultaneously by solving the above field equations as

$$\rho = -\frac{K_2(2\alpha + (c_1 + 2)r^2c_2) + 2\alpha(c_1 - 6)rh(r)h'(r) - 8\alpha c_1 h(r)^2}{32\pi(c_1^2 + c_1 - 2)K_2r^2}, \quad (37)$$

$$p = \frac{K_2(2\alpha + (c_1 + 2)r^2c_2) - 2\alpha(3c_1 + 2)rh(r)h'(r) - 8\alpha h(r)^2}{32\pi(c_1^2 + c_1 - 2)K_2r^2}, \quad (38)$$

$$E^2 = \frac{\alpha(K_2 + 2rh(r)h'(r) - 2h(r)^2)}{2(c_1 + 2)K_2r^2}. \quad (39)$$

$$(40)$$

A. Interior mode of charged gravastar

From Eqs. (37) and (38), the relation between the physical terms and the metric functions is given by

$$\rho + p = \frac{\alpha h(r)(h(r) - rh'(r))}{4\pi(c_1 + 2)K_2r^2}. \quad (41)$$

Employing the condition $\rho + p = 0$, we obtain the exact form for $h(r)$ through Eq. (41), which leads to

$$h(r) = rh_0, \quad h(r) = 0, \quad (42)$$

where h_0 acts as an integration constant. Here, $h(r) = 0$ does not provide a valid solution. On inserting the expressions of $h(r)$, the physical variables become

$$\rho = -\frac{K_2(2\alpha + (c_1 + 2)r^2c_2) - 6\alpha(c_1 + 2)r^2h_0^2}{32\pi(c_1^2 + c_1 - 2)K_2r^2} = -p, \quad (43)$$

$$E^2 = \frac{\alpha(K_2 + 2rh(r)h'(r) - 2h(r)^2)}{2(c_1 + 2)K_2r^2}, \quad (44)$$

$$\sigma = \frac{h_0\sqrt{\frac{\alpha}{(c_1+2)r^2}}}{4\sqrt{2}\pi K_2}. \quad (45)$$

The corresponding forms of lapse functions yield

$$e^a = K_1r^2, \quad e^{-b} = \frac{r^2h_0^2}{K_2}. \quad (46)$$

The active gravitational mass $M(r)$ through Eq. (37) is determined as

$$M(r) = 4\pi \left(\frac{\alpha r^3 h_0^2}{8\pi(c_1^2 + c_1 - 2)K_2} + \frac{\alpha c_1 r^3 h_0^2}{16\pi(c_1^2 + c_1 - 2)K_2} - \frac{r^3 c_2}{48\pi(c_1^2 + c_1 - 2)} - \frac{c_1 r^3 c_2}{96\pi(c_1^2 + c_1 - 2)} \right. \\ \left. - \frac{\alpha r}{16\pi(c_1^2 + c_1 - 2)} + \frac{\alpha r}{16\pi(c_1 + 2)} \right). \quad (47)$$

B. Charged gravastar shell with conformal motion

Here, we are going to compute the exact physical expressions in the light of $\rho = p$ EoS by implementing Eq. (37) and Eq. (38). $\rho = p$ is given by

$$-\frac{K_2(2\alpha + (c_1 + 2)r^2c_2) + 2\alpha(c_1 - 6)rh(r)h'(r) - 8\alpha c_1 h(r)^2}{32\pi(c_1^2 + c_1 - 2)K_2r^2} \\ = \frac{K_2(2\alpha + (c_1 + 2)r^2c_2) - 2\alpha(3c_1 + 2)rh(r)h'(r) - 8\alpha h(r)^2}{32\pi(c_1^2 + c_1 - 2)K_2r^2}. \quad (48)$$

Embedding $\rho = p$, the expression for $h(r)$ via Eq. (48) is obtained as

$$h = \frac{\sqrt{r^{-\frac{4(c_1+1)}{c_1+4}} \left(6\alpha(c_1 + 1)h_1 + 3\alpha K_2 r^{\frac{4(c_1+1)}{c_1+4}} + (c_1 + 1)K_2 c_2 r^{\frac{6(c_1+2)}{c_1+4}} \right)}}{\sqrt{6}\sqrt{\alpha(c_1 + 1)}}. \quad (49)$$

with h_1 as an integration constant. $h(r) = 0$ does not yield a valid solution. Now, substituting the forms of $h(r)$, the physical variables take the forms

$$\rho = \frac{r^{-\frac{6(c_1+2)}{c_1+4}} \left(6\alpha(c_1 + 1)(c_1 + 2)h_1 + \alpha(c_1 + 4)K_2 r^{\frac{4(c_1+1)}{c_1+4}} \right)}{16\pi(c_1 + 1)(c_1 + 2)(c_1 + 4)K_2} = p, \quad (50)$$

$$E^2 = \frac{r^{-\frac{6(c_1+2)}{c_1+4}} \left(\alpha c_1(c_1 + 4)K_2 r^{\frac{4(c_1+1)}{c_1+4}} - 6\alpha(c_1 + 1)(c_1 + 2)h_1 \right)}{2(c_1 + 1)(c_1 + 2)(c_1 + 4)K_2}, \quad (51)$$

$$\sigma = \frac{\alpha r^{-\frac{12}{c_1+4}-7} \left(6(c_1 - 2)(c_1 + 1)(c_1 + 2)h_1 + c_1(c_1 + 4)^2 K_2 r^{\frac{4(c_1+1)}{c_1+4}} \right) \sqrt{\frac{3}{c_1+1} + \frac{6h_1 r^{-\frac{4(c_1+1)}{c_1+4}}}{K_2} + \frac{r^2 c_2}{\alpha}}}{8\sqrt{3}\pi(c_1 + 1)(c_1 + 2)(c_1 + 4)^2 K_2 \sqrt{\frac{\alpha r^{-\frac{6(c_1+2)}{c_1+4}} \left(c_1(c_1 + 4)K_2 r^{\frac{4(c_1+1)}{c_1+4}} - 6(c_1 + 1)(c_1 + 2)h_1 \right)}{(c_1 + 1)(c_1 + 2)(c_1 + 4)K_2}}}. \quad (52)$$

The associated lapse functions are

$$e^a = K_1 r^2, \quad e^{-b} = \frac{1}{2c_1 + 2} + \frac{h_1 r^{-\frac{4(c_1+1)}{c_1+4}}}{K_2} + \frac{r^2 c_2}{6\alpha}. \quad (53)$$

The active gravitational mass using Eq. (37) becomes

$$M(r) = \frac{4\pi\alpha r}{16\pi c_1 + 32\pi}. \quad (54)$$

C. External mode of the charged gravastar with conformal vectors

We shall evaluate the analytic forms of physical factors using $p = \omega\rho$ EoS possessing $\omega = 0$ through Eq. (37) and Eq. (38). Considering the EoS, the expression for $h(r)$ through Eq. (48) is obtained as

$$h(r) = \frac{((3c_1 + 2)r)^{-\frac{4}{3c_1+2}} \sqrt{12\alpha h_2 + K_2((3c_1 + 2)r)^{\frac{8}{3c_1+2}} (3\alpha + 2r^2 c_2)}}{2\sqrt{3}\sqrt{\alpha}}. \quad (55)$$

in which h_2 exhibits the constant of integration. $h(r) = 0$ does not yield a consistent solution. On inserting $h(r)$, the forms of physical factors become

$$E^2 = \frac{\alpha \left(\frac{1}{c_1+2} - \frac{12h_2 r((3c_1+2)r)^{-\frac{8}{3c_1+2}-1}}{K_2} \right)}{4r^2}, \quad (56)$$

$$\sigma = \frac{\alpha((3c_1 + 2)r)^{-\frac{8}{3c_1+2}} \left((3c_1 + 2)^2 K_2 ((3c_1 + 2)r)^{\frac{8}{3c_1+2}} - 12(c_1 + 2)(3c_1 - 2)h_2 \right) \sqrt{\frac{1}{\frac{h_2((3c_1+2)r)^{-\frac{8}{3c_1+2}}}{K_2} + \frac{r^2 c_2}{6\alpha} + \frac{1}{4}}}}{8\pi(c_1 + 2)(3c_1 + 2)^2 K_2 r^3 \sqrt{\frac{\alpha \left(\frac{1}{c_1+2} - \frac{12h_2 r((3c_1+2)r)^{-\frac{8}{3c_1+2}-1}}{K_2} \right)}{r^2}}} \quad (57)$$

The lapse functions in this case are

$$e^a = K_1 r^2, \quad e^{-b} = \frac{1}{\frac{h_2((3c_1+2)r)^{-\frac{8}{3c_1+2}}}{K_2} + \frac{r^2 c_2}{6\alpha} + \frac{1}{4}}. \quad (58)$$

Now, we determine the Kretschmann scalar (K_S) to exhibit that the external mode is a flat geometry in the following form

$$K_S = R^{ijkl} R_{ijkl}, \quad (59)$$

where R indicates the Riemann tensor. The K_S for the external zone becomes,

$$K_S = \frac{\mathcal{J}_3 (144\alpha^2(3c_1(15c_1 + 4) + 52)h_0^2 + \mathcal{J}_1 + \mathcal{J}_2)}{432\alpha^4(3c_1 + 2)^2 K_2^4 r^4 ((3c_1 + 2)r)^{\frac{32}{3c_1+2}}}, \quad (60)$$

where

$$\begin{aligned} \mathcal{J}_1 &= (3c_1 + 2)^2 K_2^2 ((3c_1 + 2)r)^{\frac{16}{3c_1+2}} (45\alpha^2 + 52r^4 c_2^2 + 84\alpha r^2 c_2), \\ \mathcal{J}_2 &= 24\alpha(3c_1 + 2)h_0 K_2 ((3c_1 + 2)r)^{\frac{8}{3c_1+2}} (\alpha(45c_1 + 6) + 2(21c_1 - 10)r^2 c_2), \\ \mathcal{J}_3 &= \left(12\alpha h_0 + K_2 ((3c_1 + 2)r)^{\frac{8}{3c_1+2}} (3\alpha + 2r^2 c_2) \right)^2. \end{aligned}$$

Notice that $K_S \rightarrow 0$ as $r \rightarrow \infty$ which interprets that the external structure is an asymptotically flat geometry.

D. Boundary constraints

Boundary conditions are crucial in calculating the expressions of various parameters that arise within the system. Now, by comparing the inner and thin shell regions at the surface $r = r_1$, we derive the factor A and investigate its dependence on charge q . Additionally, by comparing the thin shell domain with the external area at $r = r_2$, we calculate the thickness $(r_2 - r_1)$ of the thin shell as well as the range of the outside radius. The internal radius is taken into account as $R_1 = 10km$ [48].

- Comparing the inner and thin shell eras at $r = r_1 = 10km$, we get:

$$K_1 r_1^2 = K_1 r_1^2, \quad (61)$$

for g_{tt} component and also for g_{rr} component, we have

$$\frac{r^2 h_0^2}{K_2} = \frac{r_1^2 r_1^{-\frac{4(c_1+1)}{c_1+4}} \left(6\alpha(c_1+1)h_1 + 3\alpha K_2 r_1^{\frac{4(c_1+1)}{c_1+4}} + (c_1+1)K_2 c_2 r_1^{\frac{6(c_1+2)}{c_1+4}} \right)}{6\alpha(c_1+1)K_2}. \quad (62)$$

- Moreover, through the thin shell and the external region at $r = r_2$, we gain

$$K_1 r_2^2 = K_1 r_2^2, \quad (63)$$

for g_{tt} component and also for g_{rr} component, we have

$$\frac{r_2^2 r_2^{-\frac{4(c_1+1)}{c_1+4}} \left(6\alpha(c_1+1)h_1 + 3\alpha K_2 r_2^{\frac{4(c_1+1)}{c_1+4}} + (c_1+1)K_2 c_2 r_2^{\frac{6(c_1+2)}{c_1+4}} \right)}{6\alpha(c_1+1)K_2} = \frac{h_2((3c_1+2)r_2)^{-\frac{8}{3c_1+2}}}{K_2} + \frac{r_2^2 c_2}{6\alpha} + \frac{1}{4}. \quad (64)$$

IV. JUNCTION CONDITIONS

Here, we match the inner and outer calculated solutions of gravastars at the hypersurface. The manifolds mathematically can be illustrated by

$$ds_{\pm}^2 = \mathcal{F}_{\pm}(r_{\pm}) dt_{\pm}^2 - \mathcal{F}_{\pm}(r_{\pm})^{-1} dr_{\pm}^2 - r_{\pm}^2 d\theta_{\pm}^2 - r_{\pm}^2 \sin^2 \theta_{\pm} d\phi_{\pm}^2, \quad (65)$$

where the metric constituents of intrinsic and extrinsic manifolds are computed with the help of field equations via boundary constraints. The lapse function of external (+) manifold can be portrayed as

$$\mathcal{F}_+(r_+) = \frac{K_2 r_+^{\frac{4(c_1+1)}{c_1+4}} ((3c_1+2)r_+)^{\frac{8}{3c_1+2}} (\alpha(6r_+^2 - 3(c_1+1)) + 2(c_1+1)(r_+^2 - 1)r_+^2 c_2)}{12\alpha(c_1+1) \left(r_+^{\frac{4(c_1+1)}{c_1+4}} - r_+^2 ((3c_1+2)r_+)^{\frac{8}{3c_1+2}} \right)}. \quad (66)$$

While for interior, we have

$$\mathcal{F}_-(r_-) = \frac{r_-^{\frac{4(c_1+1)}{c_1+4}} (6\alpha(c_1+1)h_0^2 - K_2(3\alpha + (c_1+1)r_-^2 c_2))}{6\alpha(c_1+1)}. \quad (67)$$

In the present study, the thin-shell enclosing WH geometry is created by means of a cut-and-paste method. Using this method, a unique regular manifold is produced, which can be expressed as $\mathcal{W} = \mathcal{W}^- \cup \mathcal{W}^+$. The resultant structure becomes non-singular when the shell radius is less than r_h . The components of the proposed manifolds and hypersurfaces have the following forms, according to the Israel formalism: $z_{\pm}^{\gamma} = (t_{\pm}, r_{\pm}, \theta_{\pm}, \phi_{\pm})$ and $\eta^i = (\tau, \theta, \phi)$, respectively. Here τ specifies the proper time at the hypersurface. These constituents are connected with each other with the help of the following coordinate transformation

$$g_{ij} = \frac{\partial z_{\pm}^{\gamma}}{\partial \eta^i} \frac{\partial z_{\pm}^{\delta}}{\partial \eta^j} g_{\gamma\delta}. \quad (68)$$

The parametric equation corresponding to the hypersurface is expressed by

$$\mathcal{H} : R(r, \tau) = r - y(\tau) = 0.$$

The Lanczos equations at hypersurface, which are the reduced forms of the Einstein field equations, are utilized to examine the matter axioms displayed by

$$S_{c_1}^\alpha = \frac{1}{8\pi} (\delta_{c_1}^\alpha \zeta_\gamma^\gamma - \zeta_{c_1}^\alpha), \quad (69)$$

where $\zeta_{\alpha c_1} = K_{\alpha c_1}^+ - K_{\alpha c_1}^-$ and $K_{\alpha c_1}^-$ manifest the constituents of extrinsic curvature. For perfect matter configuration, the stress-energy tensor is described as $S^\alpha_{c_1} = \text{diag}(\mathfrak{S}, \mathfrak{P}, \mathfrak{P})$. The surface density and pressure at shell are expressed by \mathfrak{S} and \mathfrak{P} , respectively. The extrinsic curvatures for inner and outer geometries are

$$K_{\alpha c_1}^\pm = -n_\mu^\pm \left[\frac{\partial^2 z_\pm^\mu}{\partial \eta^\alpha \partial \eta^{c_1}} + \Gamma_{\lambda\nu}^\mu \left(\frac{\partial z_\pm^\lambda}{\partial \eta^\alpha} \right) \left(\frac{\partial z_\pm^\nu}{\partial \eta^{c_1}} \right) \right]. \quad (70)$$

The unit normals become

$$n_\pm^\mu = \left(\frac{\dot{y}}{\mathcal{F}_\pm(y)}, \sqrt{\dot{y}^2 + \mathcal{F}_\pm(y)}, 0, 0 \right), \quad (71)$$

in which the overdot indicates the differential associated with proper time.

Employing Lanczos equations, we obtain

$$\mathfrak{S} = -\frac{[K_\theta^\theta]}{4\pi} = -\frac{1}{4\pi y} \left\{ \sqrt{\dot{y}^2 + \mathcal{F}_+(y)} - \sqrt{\dot{y}^2 + \mathcal{F}_-(y)} \right\}, \quad (72)$$

$$\mathfrak{P} = \frac{[K_\theta^\theta] + [K_\tau^\tau]}{8\pi} = \frac{1}{8\pi y} \left\{ \frac{2\dot{y}^2 + 2y\dot{y} + 2\mathcal{F}_+(y) + y\mathcal{F}'_+(y)}{\sqrt{\dot{y}^2 + \mathcal{F}_+(y)}} - \frac{2\dot{y}^2 + 2y\dot{y} + 2\mathcal{F}_-(y) + y\mathcal{F}'_-(y)}{\sqrt{\dot{y}^2 + \mathcal{F}_-(y)}} \right\}. \quad (73)$$

It is assumed that the thin shell of the generated geometry has no movement in a radial direction at equilibrium shell radius y_0 . Hence, it is observed that the proper time differential of shell radius disappears, i.e., $y_0 = 0 = \dot{y}_0$.

$$\mathfrak{S}_0 = -\frac{1}{4\pi y_0} \left\{ \sqrt{\mathcal{F}_+(y_0)} - \sqrt{\mathcal{F}_-(y_0)} \right\}, \quad (74)$$

$$\mathfrak{P}_0 = \frac{1}{8\pi y_0} \left\{ \frac{2\mathcal{F}_+(y_0) + y_0\mathcal{F}'_+(y_0)}{\sqrt{\mathcal{F}_+(y_0)}} - \frac{2\mathcal{F}_-(y_0) + y_0\mathcal{F}'_-(y_0)}{\sqrt{\mathcal{F}_-(y_0)}} \right\}, \quad (75)$$

where at equilibrium position, density and pressure are presented by $\mathfrak{S}(y_0)$ and $\mathfrak{P}(y_0)$, respectively.

V. STABILITY VIA LINEARIZED RADIAL PERTURBATION

We now going to discuss the stable state of a created thin-shell about WH geometry via linearized radial perturbation at $y = y_0$. We obtain the equation of motion of the shell through Eq. (72) given by

$$\Pi(y) + \dot{y}^2 = 0, \quad (76)$$

having $\Pi(y)$ as effective potential function illustrated by

$$\Pi(y) = -\frac{(\mathcal{F}_-(y) - \mathcal{F}_+(y))^2}{64\pi^2 y^2 \mathfrak{S}(y)^2} + \frac{1}{2} (\mathcal{F}_-(y) + \mathcal{F}_+(y)) - 4\pi^2 y^2 \mathfrak{S}(y)^2. \quad (77)$$

It is interesting that the constituents of the stress-energy tensor obey the energy conservation requirements given by

$$\frac{d}{d\tau} (4\pi y^2 \mathfrak{S}(y)) + \mathfrak{P}(y) \frac{d}{d\tau} (4\pi y^2) = 0, \quad (78)$$

which yields

$$\mathfrak{S}'(y) = -\frac{\mathfrak{P}(\mathfrak{S}(y)) + 2(\mathfrak{S}(y))}{y}. \quad (79)$$

In order to expand the effective potential around the equilibrium shell radius to second-order factors for stable geometry, we implement the Taylor expansion given by

$$\Pi(y) = \Pi(y_0) + (y - y_0)\Pi'(y_0) + \frac{1}{2}(y - y_0)^2\Pi''(y_0) + O[(y - y_0)^3]. \quad (80)$$

The resulting geometry becomes stable for $\Pi(y_0) = 0 = \Pi'(y_0)$. Thus, we obtain

$$\Pi(y) = \frac{1}{2}(y - y_0)^2\Pi''(y_0). \quad (81)$$

To manifest the stability of thin-shell, the second differential form of the effective potential at $y = y_0$ can be implemented as

- Unstable $\Rightarrow \Pi''(y_0) < 0$,
- Stable $\Rightarrow \Pi''(y_0) > 0$,
- Unpredictable $\Rightarrow \Pi''(y_0) = 0$.

$$\begin{aligned} \Pi''(y_0) = & \left(y_0\mathfrak{S}(y_0) \left(y_0\mathfrak{S}(y_0) \left(16\pi^2\mathcal{A}_2y_0^2\mathfrak{S}(y_0)^2 - (\mathcal{F}'_-(y_0) - \mathcal{F}'_+(y_0))^2 \right) - \mathcal{A}_4\mathcal{F}_-(y_0) \right) \right. \\ & \left. + \mathcal{F}_+(y_0) (\mathcal{A}_3y_0\mathfrak{S}(y_0) - 2\mathcal{A}_5\mathcal{F}_-(y_0)) + \mathcal{A}_5\mathcal{F}_-(y_0)^2 + \mathcal{A}_1\mathcal{F}_+(y_0)^2 \right) (32\pi^2y_0^4\mathfrak{S}(y_0)^4)^{-1}, \end{aligned} \quad (82)$$

where

$$\begin{aligned} \mathcal{A}_1 &= 3\mathfrak{S}(y_0)(2\mathfrak{P}(y_0) + \mathfrak{S}(y_0)) - 4(\mathfrak{P}(y_0) + \mathfrak{S}(y_0))(-\mathfrak{S}(y_0)\mathfrak{P}'(y_0) + 3\mathfrak{P}(y_0) + \mathfrak{S}(y_0)), \\ \mathcal{A}_2 &= \mathcal{F}''_-(y_0) + \mathcal{F}''_+(y_0) + 16\pi^2(\mathfrak{S}(y_0)(2\mathfrak{P}(y_0) + \mathfrak{S}(y_0)) - 4(\mathfrak{P}(y_0) + \mathfrak{S}(y_0))(\mathfrak{S}(y_0)(\mathfrak{P}'(y_0) + 1) + \mathfrak{P}(y_0))), \\ \mathcal{A}_3 &= 8\mathfrak{P}(y_0)(\mathcal{F}'_-(y_0) - \mathcal{F}'_+(y_0)) + \mathfrak{S}(y_0)(y_0\mathcal{F}''_-(y_0) + 4\mathcal{F}'_-(y_0) - y_0\mathcal{F}''_+(y_0) - 4\mathcal{F}'_+(y_0)), \\ \mathcal{A}_4 &= 8\mathfrak{P}(y_0)(\mathcal{F}'_-(y_0) - \mathcal{F}'_+(y_0)) + \mathfrak{S}(y_0)(y_0\mathcal{F}''_-(y_0) + 4\mathcal{F}'_-(y_0) - y_0\mathcal{F}''_+(y_0) - 4\mathcal{F}'_+(y_0)), \\ \mathcal{A}_5 &= 4\mathfrak{S}(y_0)(\mathfrak{P}(y_0) + \mathfrak{S}(y_0))\mathfrak{P}'(y_0) - 10\mathfrak{P}(y_0)\mathfrak{S}(y_0) - 12\mathfrak{P}(y_0)^2 - \mathfrak{S}(y_0)^2. \end{aligned}$$

A. Phantomlike EoS

The stable thin-shell configuration is a highly significant subject in the realms of astrophysics and cosmology, since it assists in the inspection of valid gravastar results. EoS is essential for examining the impacts of distinct kinds of matter constituents at the hypersurface on the stable state of a thin shell. Among various speculations that can narrate the exotic substance, one is a phantom-like EoS, that is portrayed as

$$\mathfrak{P} = \omega\mathfrak{S}(y), \quad (83)$$

where the parameter of EoS $\omega < 0$. The various bounds of EoS parameter characterize the distinct kinds of matter constituents. It exhibits dark energy, quintessence, and phantom energy state if $\omega < -1/3$, $0 > \omega > -1/3$ and $\omega < -1$, respectively. To explore the thin-shell stability for three distinct forms of EoS parameter, i.e., dark energy, quintessence, and phantom energy like matter constituents, we observe the graphical behavior of the second derivative of effective potential as presented in Eq. (82). For simplification, we can consider $y = (S_0^m + \ell^m)^{1/m}$, in which ℓ depicts the length factor and m acts as a constant. We scrutinize the outcome of distinct factors on the stable state of the shell for different types of energy contents. Some detailed outcomes are given below:

- Figs. (1)-(3) are used to explore the impact of c_1 on the stability of gravastars for dark, quintessence and phantom energies, respectively. Here, we use the regional plots to portray the stable and unstable states of the shell. The stable regions are denoted with the pink dotted region and the unstable region is represented with

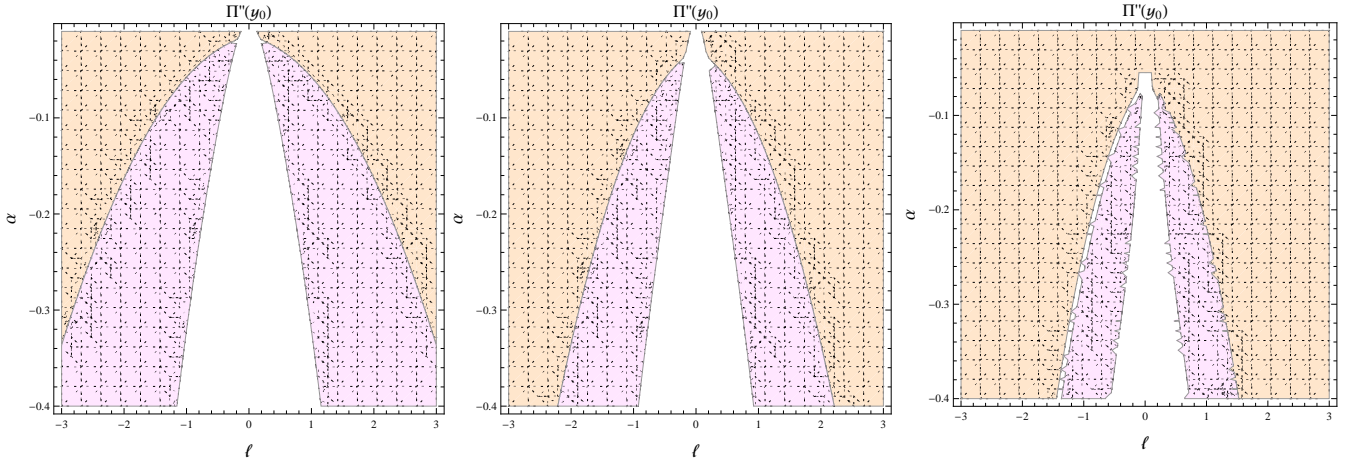


FIG. 1: Plots of $\Pi''(y_0)$ along α and ℓ for dark energy for various choices of c_1 as $c_1 = 0.3$ (first plot), $c_1 = 0.5$ (second plot) and $c_1 = 0.9$ (third plot) for $\omega = -1$, $y_0 = (l^m + 1)^{1/m}$, $h_0 = 1$, $K_2 = 0.1$, $c_2 = 0.5$, $m = 2$.

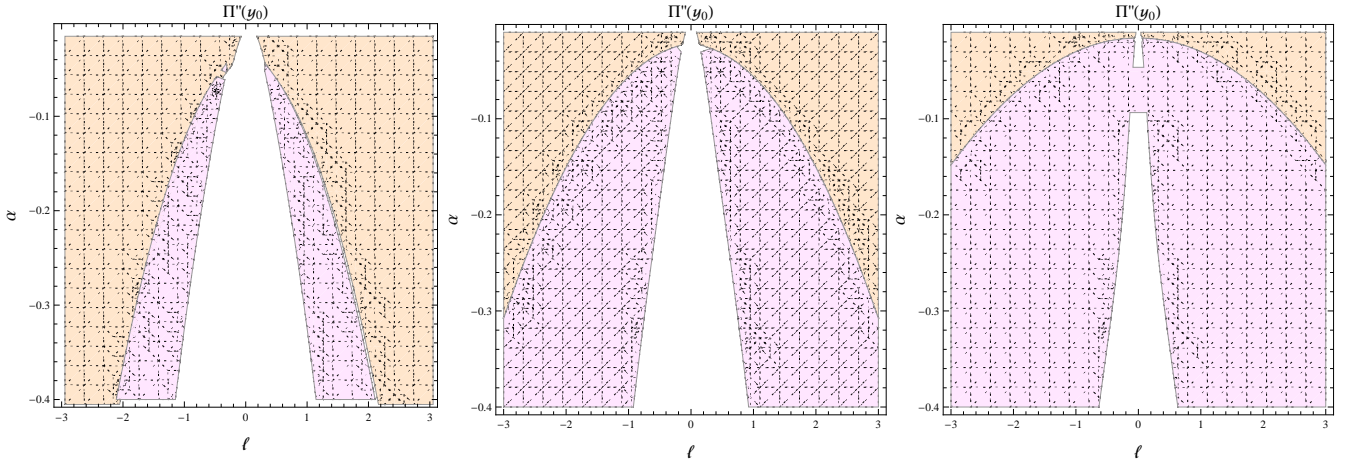


FIG. 2: Plots of $\Pi''(y_0)$ along α and ℓ for quintessence energy for various choices of c_1 as $c_1 = 0.3$ (first plot), $c_1 = 0.5$ (second plot) and $c_1 = 0.9$ (third plot) for $\omega = -2/3$, $y_0 = (l^m + 1)^{1/m}$, $h_0 = 1$, $K_2 = 0.1$, $c_2 = 0.5$, $m = 2$.

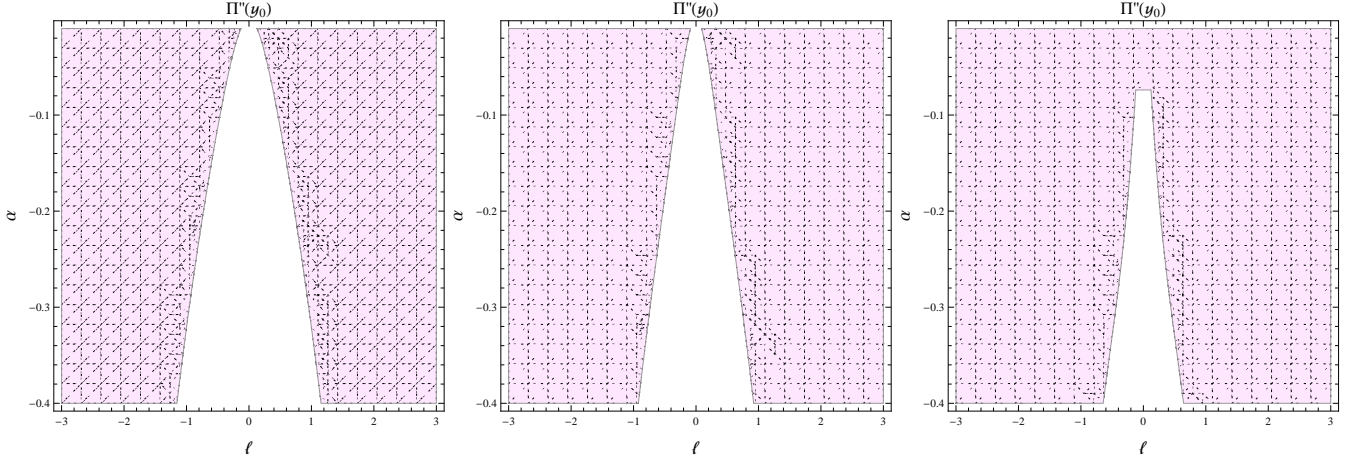


FIG. 3: Plots of $\Pi''(y_0)$ along α and ℓ for phantom energy for various choices of c_1 as $c_1 = 0.3$ (first plot), $c_1 = 0.5$ (second plot) and $c_1 = 0.9$ (third plot) for $\omega = -2$, $y_0 = (l^m + 1)^{1/m}$, $h_0 = 1$, $K_2 = 0.1$, $c_2 = 0.5$, $m = 2$.

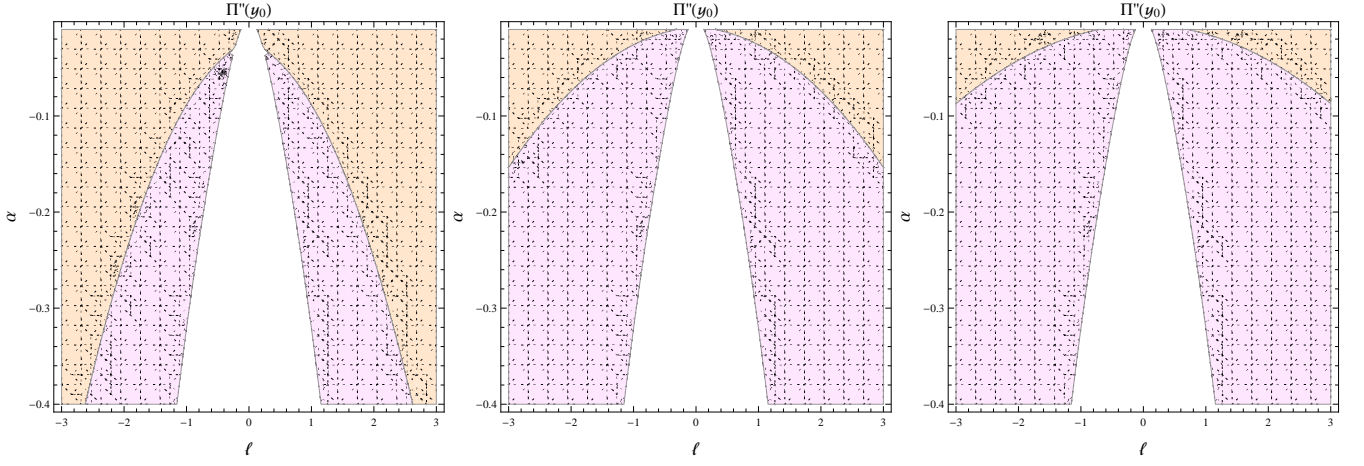


FIG. 4: Plots of $\Pi''(y_0)$ for dark energy for $h_0 = 0.8$ (first plot), $h_0 = 1.5$ (second plot) and $h_0 = 2$ (third plot) for $\omega = -1$, $y_0 = (l^m + 1)^{1/m}$, $c_1 = 0.3$, $K_2 = 0.1$, $c_2 = 0.5$, $m = 2$.

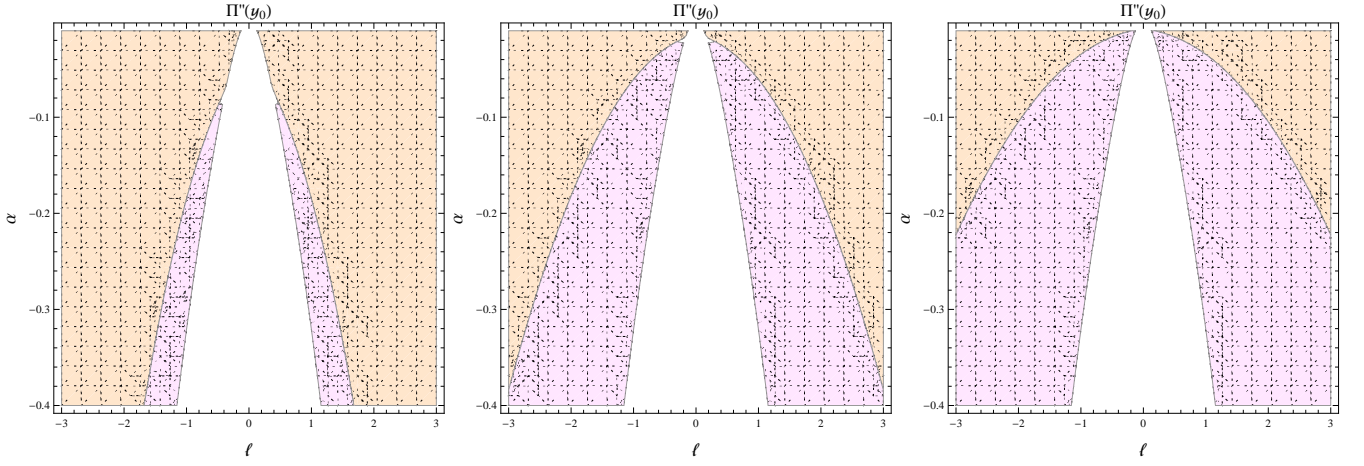


FIG. 5: Plots of $\Pi''(y_0)$ for quintessence energy for $h_0 = 0.8$ (first plot), $h_0 = 1.5$ (second plot) and $h_0 = 2$ (third plot) for $\omega = -2/3$, $y_0 = (l^m + 1)^{1/m}$, $c_1 = 0.3$, $K_2 = 0.1$, $c_2 = 0.5$, $m = 2$.

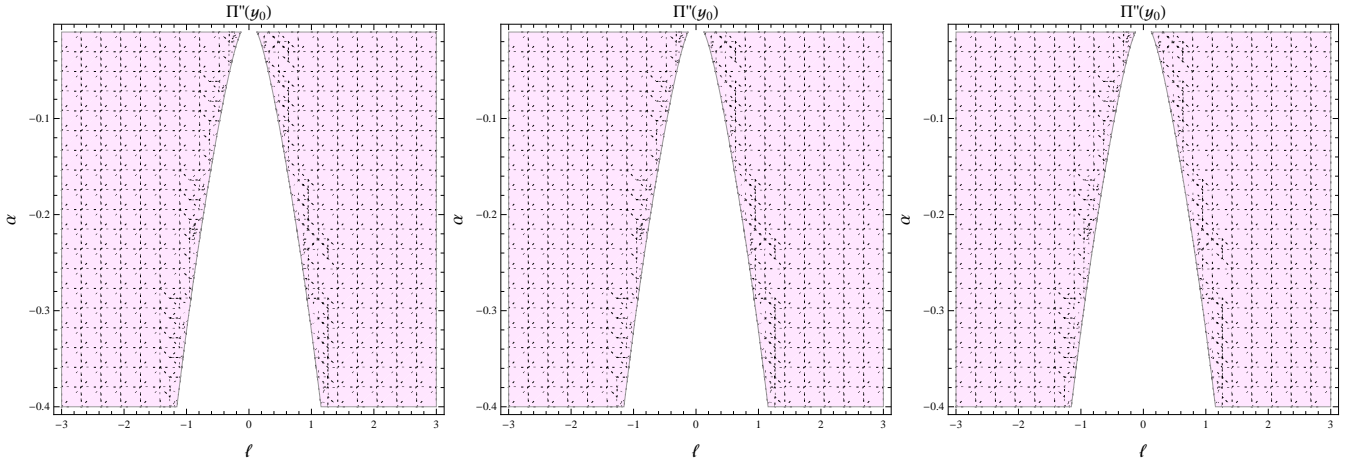


FIG. 6: Plots of $\Pi''(y_0)$ for phantom energy for $h_0 = 0.8$ (first plot), $h_0 = 1.5$ (second plot) and $h_0 = 2$ (third plot) for $\omega = -2$, $y_0 = (l^m + 1)^{1/m}$, $c_1 = 0.3$, $K_2 = 0.1$, $c_2 = 0.5$, $m = 2$.

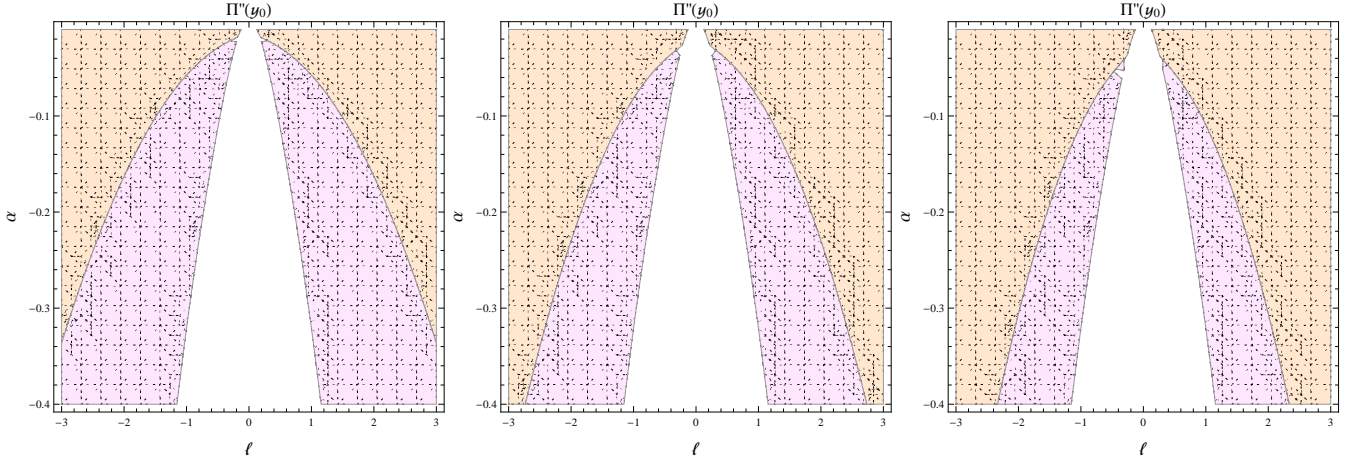


FIG. 7: Plots of $\Pi''(y_0)$ for dark energy for $K_2 = 0.1$ (first plot), $K_2 = 0.12$ (second plot) and $K_2 = 0.14$ (third plot) for $\omega = -1, y_0 = (l^m + 1)^{1/m}, c_1 = 0.3, h_0 = 1, c_2 = 0.5, m = 2$.

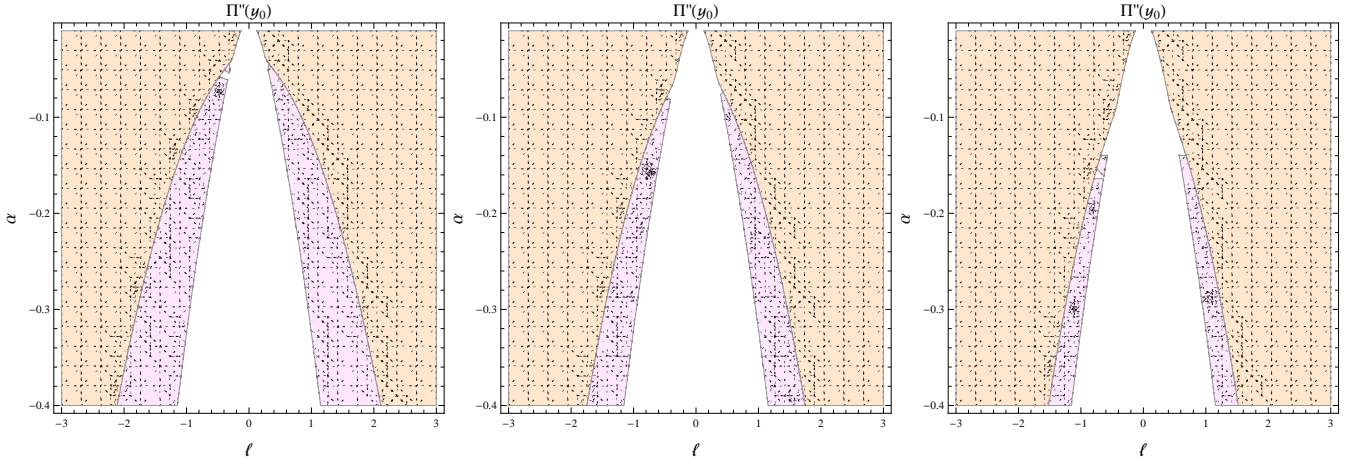


FIG. 8: Plots of $\Pi''(y_0)$ for quintessence energy for $K_2 = 0.1$ (first plot), $K_2 = 0.12$ (second plot) and $K_2 = 0.14$ (third plot) for $\omega = -2/3, y_0 = (l^m + 1)^{1/m}, c_1 = 0.3, h_0 = 1, c_2 = 0.5, m = 2$.

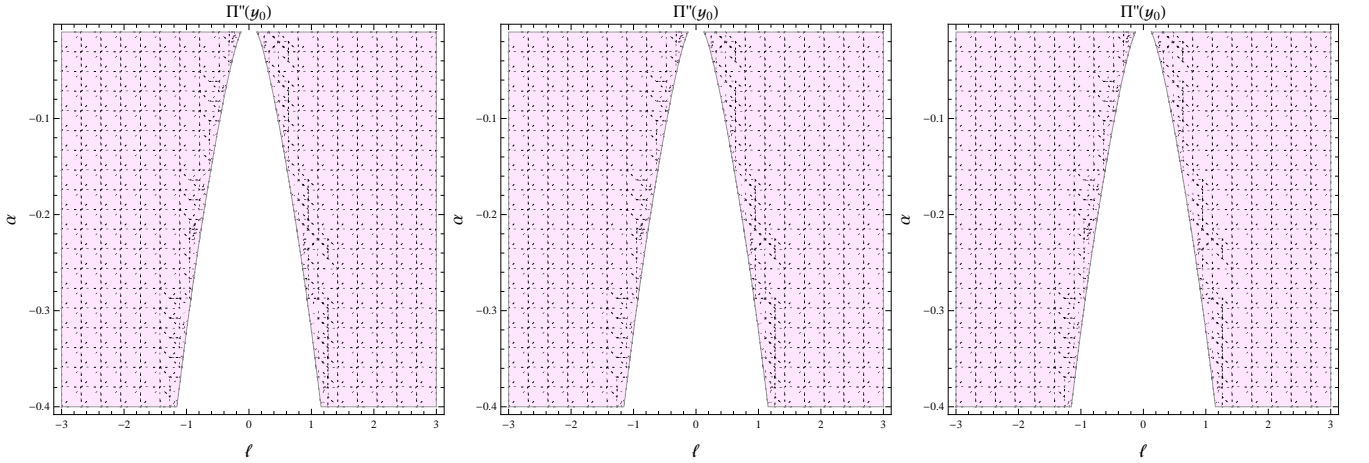


FIG. 9: Plots of $\Pi''(y_0)$ for phantom energy for $K_2 = 0.1$ (first plot), $K_2 = 0.12$ (second plot) and $K_2 = 0.14$ (third plot) for $\omega = -2, y_0 = (l^m + 1)^{1/m}, c_1 = 0.3, h_0 = 1, c_2 = 0.5, m = 2$.

the grey dotted region. It is noted that the stability is reduced by increasing the parameter c_1 for the dark energy distributions see Fig. (1). In the presence of quintessence energy, this parameter behaves differently. For such matter contents, the stability regions become greater for higher values of c_1 see Fig. (2). For the phantom energy, the created geometry displays maximal stable nature for smaller as well as higher values of c_1 as compared to the dark as well as quintessence energy contents see Fig. (3).

- Figs. (4)-(6) are used to observe the stable/unstable phase of the obtained structure for different choices of h_0 having distinct kinds of matter contents. For the selection of dark and quintessence matter distribution, the developed structure expresses maximum stable behavior for greater choices of h_0 see Fig. (4) and (5). For the phantom energy, the gained structure only exhibits stable conduct and the stable regions increase by increasing h_0 .
- Figs.(7)-(9) are devoted to explain the impact of K_2 . It is noted that the smaller values of K_2 are only suitable for the stable behavior of the gravastar structure see Fig.(7). For phantom energy system shows more unstable behavior as compared to the dark energy see Fig.(8). For the phantom energy again system is expresses maximum stable behavior for every choice of the K_2 see Fig.(9).

VI. SOME PHYSICAL ATTRIBUTES

The physical properties of charged gravastars like appropriate length, energy, and entropy with CKVs, are the main topics of this section. The shell's proper length, denoted by δ , and thickness are discussed here. The thickness of the shell is a tiny real positive value, δ , such that $0 < \delta \ll 1$. The parameters y and $y + \delta$ specify the shell's bounds. The appropriate length of the shell is displayed mathematically as follows [49]

$$l = \int_y^{y+\delta} \sqrt{e^{\mathcal{Y}(r)}} = \int_y^{y+\delta} \sqrt{\frac{K_2 r^{\frac{4(c_1+1)}{c_1+4}} ((3c_1+2)r)^{\frac{8}{3c_1+2}} (\alpha(6r^2-3(c_1+1)) + 2(c_1+1)(r^2-1)r^2c_2)}{12\alpha(c_1+1) \left(r^{\frac{4(c_1+1)}{c_1+4}} - r^2((3c_1+2)r)^{\frac{8}{3c_1+2}} \right)}} dr. \quad (84)$$

To resolve the aforementioned intricate integration, we presume that the

$$\sqrt{\frac{K_2 r^{\frac{4(c_1+1)}{c_1+4}} ((3c_1+2)r)^{\frac{8}{3c_1+2}} (\alpha(6r^2-3(c_1+1)) + 2(c_1+1)(r^2-1)r^2c_2)}{12\alpha(c_1+1) \left(r^{\frac{4(c_1+1)}{c_1+4}} - r^2((3c_1+2)r)^{\frac{8}{3c_1+2}} \right)}} = \frac{dB(r)}{dr}, \quad (85)$$

as

$$\begin{aligned} l &= \int_y^{y+\delta} \frac{dB(r)}{dr} dr = B(y+\delta) - B(y) \approx \delta \frac{dB(r)}{dr} \Big|_{r=y} \\ &= \delta \sqrt{\frac{K_2 y^{\frac{4(c_1+1)}{c_1+4}} ((3c_1+2)y)^{\frac{8}{3c_1+2}} (\alpha(6y^2-3(c_1+1)) + 2(c_1+1)(y^2-1)y^2c_2)}{12\alpha(c_1+1) \left(y^{\frac{4(c_1+1)}{c_1+4}} - y^2((3c_1+2)y)^{\frac{8}{3c_1+2}} \right)}}. \end{aligned} \quad (86)$$

δ is a small real positive constant whose square and higher powers can be neglected. The shell's thickness and the proper length can therefore be correlated and examined. Both the shell radius and the physical parameters influence this relationship. It is found that the proper length of the shell increases by increasing the shell's thickness see Fig. (10). Also, the physical parameter α greatly affects the proper length. It is noted that the proper length becomes smaller by enhancing α negatively. Also, this graphical analysis explains the direct relation between the proper length and thickness of the shell. It is also observed that the parameter affects the proper length. It is found that the proper becomes greater by enhancing the parameter c_1 see the right plot of Fig. (10).

A non-attractive force and a negative energy zone exist in the internal region of a gravastar, because the substance follows the equation of state $p = -\rho$. Finding the appropriate length as [49]

$$\mathbf{E} = \int_y^{y+\delta} 4\pi r^2 \rho(r) dr = \delta \frac{\alpha y^{-\frac{4(c_1+1)}{c_1+4}} \left(6(c_1^2 + 3c_1 + 2)h_1 + (c_1 + 4)K_2 y^{\frac{4(c_1+1)}{c_1+4}} \right)}{4(c_1+1)(c_1+2)(c_1+4)K_2^2}. \quad (87)$$

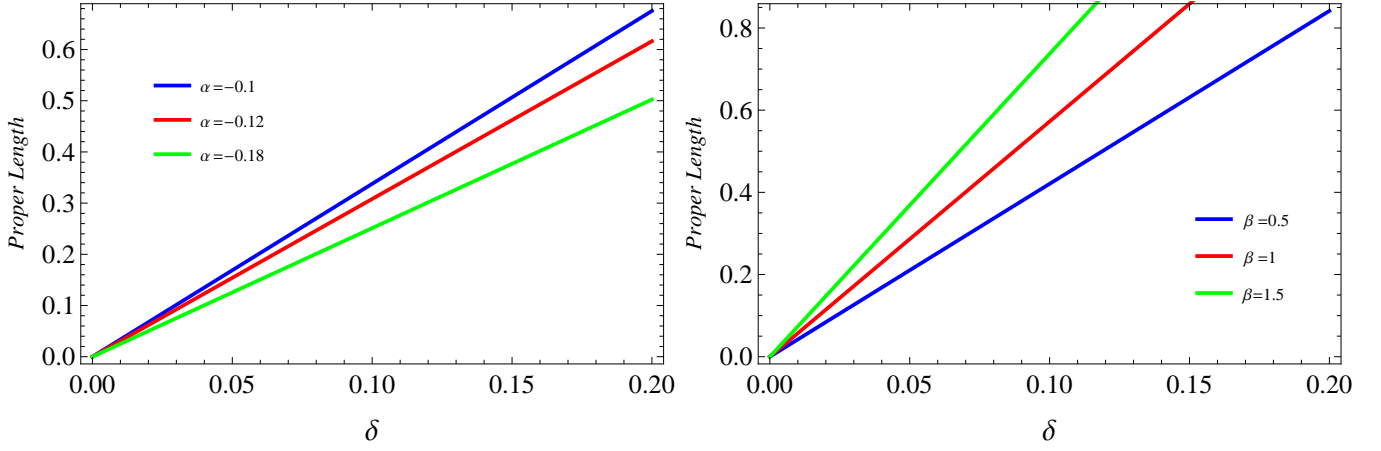


FIG. 10: Proper length along δ for various choices of α (left plot) and c_1 (right plot) with $h_1 = 1, \alpha = 0.5, Y = 0.5, c_2 = 1, z = 10$;

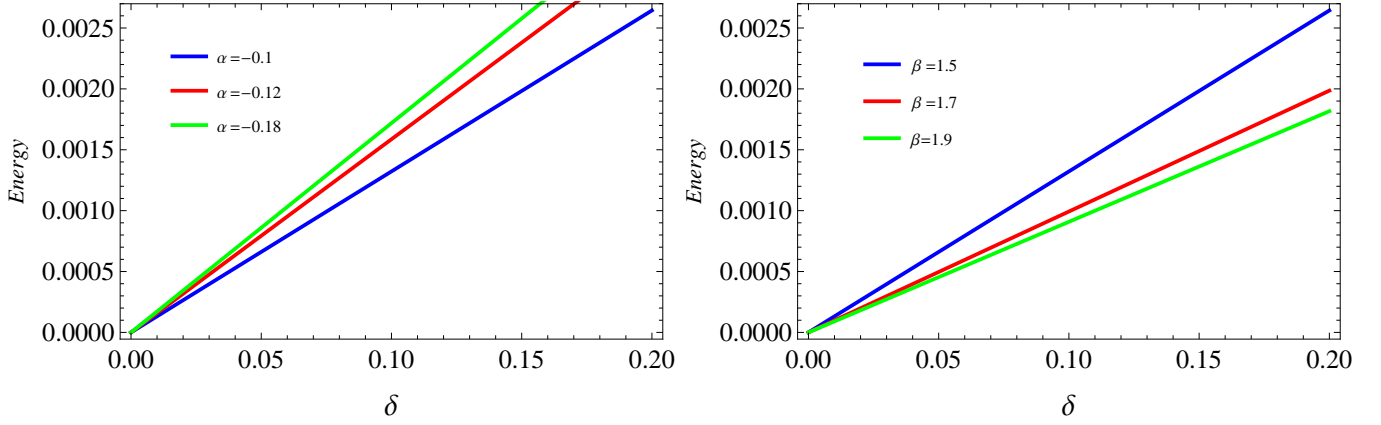


FIG. 11: Energy contents along δ for various choices of α (left plot) and c_1 (right plot) with $h_1 = 1, \alpha = 0.5, Y = 0.5, c_2 = 1, z = 10$;

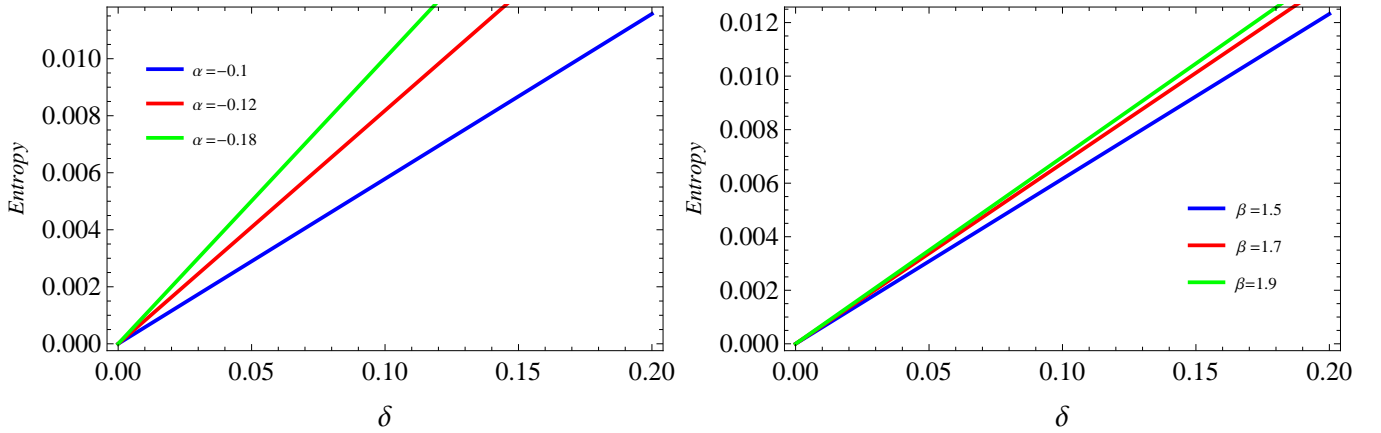


FIG. 12: Entropy of shell along δ for distinct choices of α (left plot) and c_1 (right plot) with $h_1 = 1, \alpha = 0.5, Y = 0.5, c_2 = 1, z = 10$;

The final shell energy expression is dependent on the physical parameters of gravity and the thickness and radius of the shell.

It is found that the energy of the shell reduces by enhancing the shell's thickness see Fig. (11). Also, the physical parameter α greatly affects the energy. It is noted that the energy becomes larger as α increases negatively. Also, this graphical analysis explains the inverse relation between the energy of the shell and the c_1 . For higher values of c_1 , the energy of the shell becomes smaller see the right plot of Fig. (11).

The degree of disturbance or disruption in a structure of geometry is able to be determined using the amount of entropy of the structure. To measure the randomness of gravastar, the shell's entropy is examined. Mazur and Mottola's concept is utilized to get the entropy equation of a gravastar thin-shell as [49]

$$S = \int_y^{y+\delta} 4\pi r^2 j(r) \sqrt{e^{Y(r)}} dr. \quad (88)$$

The entropy density at a given local temperature is computed as

$$j(r) = \frac{\eta K_B}{\hbar} \sqrt{\frac{p(r)}{2\pi}}, \quad (89)$$

with η as a dimensionless factor. Here, we consider Planck units ($K_B = 1 = \hbar$) yielding the following form of the shell's entropy [49]

$$S = \delta \frac{y^2 \sqrt{\frac{-\frac{6(c_1+2)}{c_1+4} \left(6\alpha(c_1+1)(c_1+2)h_1 + \alpha(c_1+4)K_2 y^{\frac{4(c_1+1)}{c_1+4}} \right)}{(c_1+1)(c_1+2)(c_1+4)K_2}}}{2\sqrt{6} \sqrt{\frac{K_2 y^{\frac{4(c_1+1)}{c_1+4}} \left((3c_1+2)y^{\frac{8}{3c_1+2}} (\alpha(6y^2-3(c_1+1))+2(c_1+1)(y^2-1)y^2 c_2) \right)}{\alpha(c_1+1) \left(y^{\frac{4(c_1+1)}{c_1+4}} - y^2((3c_1+2)y)^{\frac{8}{3c_1+2}} \right)}}}}. \quad (90)$$

Moreover, the shell's entropy should be proportional to δ . It is gained that the energy of the shell reduces by enhancing the shell's thickness see Fig. (12). It is noted that the entropy of the shell increases by enhancing α negatively. For higher values of c_1 , the entropy of the shell becomes larger.

VII. CONCLUSION

In this paper, we scrutinize the gravastar geometry in $f(\mathcal{T}, T)$ gravity, an extended teleparallel gravity with spherically symmetric space-time and an isotropic fluid source. By using the conformal symmetry for the spherically symmetric space-time, we want to investigate gravastar. As far as we are aware, this is the initial effort to look into the gravastar $f(\mathcal{T}, T)$ theory. To sum up, the investigation of gravastar geometry has uncovered discrete areas with disparate equations of state ($p = \omega\rho$, where $\omega = -1, 1, 0$) and conformal coordinates of death. The Kretschmann scalar confirmed regularity and the determination of precise solutions for the interior, intermediate, and outer areas. Gravastars' overall geometry was formed by joining these regions with junction conditions, taking into account two possible external geometry possibilities. The stability and physical properties of charged gravastars were investigated; stability restrictions in terms of the coupling constant and conformal parameters were discussed. The assessment of the produced structure's appropriate length, energy content, and entropy adds to our knowledge about gravastars and their characteristics. The detail discussion are given below:

- The stability of gravastars is closely connected to the parameters c_1 , h_0 , and K_2 , which represent the specific sort of energy content within the system see Figs. (1)-(9). The behavior of gravastar structures exhibited substantial variations depending on the dominant presence of either dark, quintessence, or phantom energy. Increasing the value of c_1 generally decreases the stability of dark energy, but it improves the stability of quintessence energy and results in the highest level of stability for phantom energy. Similarly, larger values of h_0 enhanced stability in structures containing dark and quintessence energy, whereas structures with phantom energy remain stable regardless of the chosen value of h_0 . Furthermore, it has been observed that gravastar structures tend to be more stable when the values of K_2 are lower. In particular, systems with phantom energy show higher levels of instability compared to systems with dark energy. These findings emphasize the intricate interaction among many energy components and characteristics in affecting the stability of gravastars.
- The association between the shell thickness and its suitable length has been analyzed in detail; physical characteristics and the shell radius are important factors in defining this correlation. As shown in Fig. (10), it is

seen that the shell's proper length increases with the shell's thickness. The proper length is strongly influenced by the physical parameter α ; a negative rise in α results in a drop in the proper length. Furthermore, as can be observed in the right plot of Fig. (10), the parameter c_1 also influences the proper length, with larger values resulting in a longer proper length. Moreover, as the thickness increases, the shell's energy drops, as shown in Fig. (11), where α and c_1 are critical factors in determining the energy levels. Based on Fig. (12), it is determined that the shell's entropy is proportional to δ , increasing with a negative enhancement in α and for greater values of c_1 .

These results offer important new understandings of how shell parameters and physical attributes interact to define the shell's properties within gravastar structures.

Acknowledgement

F. Javed greets the financial assistance received for his postdoctoral fellowship under Grant No. YS304023917 at Zhejiang Normal University.

References

-
- [1] Mazur, P. and Mottola, E.: Proc. Natl. Acad. Sci. USA **101**(2004)9545.
 - [2] Chapline, G. et al.: Int. J. Mod. Phys. A **18**(2003)3587.
 - [3] Visser, M. and Wiltshire, D.L.: Class. Quantum Grav. **21**(2004)1135.
 - [4] Carter, B.M.N.: Class. Quantum Grav. **22**(2005)4551.
 - [5] Bilić, N., Tupper, G.B. and Viollier, R.D.: J. Cosmol. Astropart. Phys. **02**(2006)013.
 - [6] Horvat, D. and Ilijić, S.: Class. Quantum Grav. **24**(2007)5637.
 - [7] M. Sharif, and F. Javed.: Annals of Physics 415 (2020)168124; Eur. Phys. J. C 81 (2021)1-11.
 - [8] Sharif, M. and Javed, F.: Journal of Experimental and Theoretical Physics 132.3 (2021)381-393; Journal of Experimental and Theoretical Physics, 133(4)(2021)439-448.
 - [9] Sharif, M. and Javed, F.: Astrophysics and Space Science 366.11 (2021) 103; Chin. J. Phys. 77 (2022)804-815.
 - [10] Javed, F., Mumtaz, S., Mustafa, G., Atamurotov, F., and Ghosh, S. G.: Chinese Journal of Physics 88(2024)55-68.
 - [11] Chirenti, C.B.M.H. and Rezzolla, L. Class. Quantum Grav. **24**(2007)4191.
 - [12] Rocha, P. et al.: J. Cosmol. Astropart. Phys. **11**(2008)010.
 - [13] Harko, T., Kovács, Z. and Lobo, F.S.N.: Class. Quantum Grav. **26**(2009)215006.
 - [14] Lobo, F.S.N. and Arellano, A.V.B.: Class. Quantum Grav. **24**(2007)1069.
 - [15] Horvat, D., Ilijić, S. and Marunovic, A.: Class. Quantum Grav. **26**(2009)025003.
 - [16] Turimov, B.V., Ahmedov, B.J. and Abdujabbarov, A.A.: Mod. Phys. Lett. A **24**(2009)733.
 - [17] Javed, F. and Lin, J.: Chin. J. Phys. **88**(2024)786.
 - [18] Sharif, M. and Javed, F.: Astronomy Reports **65.5** (2021)353-361.
 - [19] Waseem, A. et al.: Eur. Phys. J. C **83.11** (2023)1088.
 - [20] Javed, F., A. Waseem, G. Mustafa, and E. Güdekli. Int. J. Geo. Methods Mod. Phys. **21**, no. 3 (2024): 2450061-77.
 - [21] Javed, F.: Annals of Physics **458** (2023)169464.
 - [22] Javed, F. Waseem, A., Lin, J., Sadiq, S., Mustafa, G., Alshehri, M.H.: Eur. Phys. J. C **84.3** (2024)337.
 - [23] Javed, F.: Eur. Phys. J. C **83.6** (2023)513.
 - [24] Harko, T. et al.: Phys. Rev. D **84**(2011)024020.
 - [25] Haghani, Z. et al.: Phys. Rev. D **88**(2013)044023; Odintsov, S.D. and Sáez-Gómez, D.: Phys. Lett. B **725**(2013)437.
 - [26] Sharif, M. and Ikram, A.: Eur. Phys. J. C **76**(2016)640.
 - [27] Harko, T. et al.: J. Cosmol. Astropart. Phys. **12**(2014)021.
 - [28] Das, A. et al.: Phys. Rev. D **95**(2017)124011.
 - [29] Shamir, F. and Ahmad, M.: Phys. Rev. D **97**(2018)104031.
 - [30] Sharif, M. and Waseem, A.: Eur. Phys. J. Plus **135**(2020)930.
 - [31] Sharif, M. and Naz, S.: Mod. Phys. Lett. A **37**(2022)2250125.
 - [32] Sharif, M. and Naz, S.: Mod. Phys. Lett. A **37**(2022)2250065.
 - [33] Ghosh, S. et al.: Int. J. Mod. Phys. A **35**(2020)2050017.
 - [34] Usmani, A.A. et al.: Phys. Lett. B **701**(2011)388.
 - [35] Sharif, M. and Waseem, A.: Astrophys. Space Sci. **364**(2019)189.
 - [36] Bhar, P. and Rej, P.: Int. J. Geom. Meth. Mod. Phys. **18**(2021)2150112.
 - [37] Sharif, M. and Saeed, M.: Chin. J. Phys. **77**(2022)583.

- [38] Sharif, M. and Naz, S.: Eur. Phys. J. Plus **137**(2022)421.
- [39] Das A, Ghosh S, Deb D, Rahaman F, Ray S.: Nuclear Physics B. 954(2020)114986.
- [40] Sengupta R, Ghosh S, Ray S, Mishra B, Tripathy SK. Physical Review D. 2020 Jul 10;102(2):024037.
- [41] Ray S, Ghosh S, Sengupta R.: Modern Physics Letters A. 21;37(29)(2022)2250195.
- [42] Bhar, P.: arXiv:2404.05761v1.
- [43] Javed, F., Waseem, A., Mustafa, G., Atamurotov, F., Ahmedov, B., Abdujabbarov, A.: arXiv:2403.01405v1.
- [44] Mohanty, D., Ghosh, S., and Sahoo, P.K.: Annals of Physics (2024): 169636.
- [45] Debadri, B, and Chattopadhyay, P. K.: arXiv preprint arXiv:2401.14061 (2024).
- [46] M. Pace, J. Levi Said, Eur. Phys. J. C 2017, 77, 62.
- [47] M. Pace, J. Levi Said, Eur. Phys. J. C 2017, 77, 283.
- [48] Ghosh, S., Ray, S., Rahaman, F. and Guha, B.K.: Ann. Phys. **394**(2018)230.
- [49] Ghosh, S., Rahaman, F., Guha, B.K. and Ray, S.: Phys. Lett. B **767**(2017)380.